NATIONAL REMOTE SENSING CENTRE
REPORT / DOCUMENT CONTROL SHEET

1.	Security Classification	Unclassified		
2.	Distribution	Through soft and hard copies		
3.	Report / Document version	**(a) Issue no.:**02		**(b) Revision & Date:** R01/ Nov 2017
4.	Report / Document Type	Technical Report		
5.	Document Control Number	NRSC-ECSA-OIBMD-JAN-2018-TR-1099 1.0		
6.	Title	Ocean Surface Currents for Global Ocean		
7.	Particulars of collation	**Pages: 18**	**Figures: 12**	**References: 20**
8.	Author (s)	Shashank Kr Mishra[1],		
9.	Affiliation of authors	[1] OIBMD, ECSA, NRSC, Hyderabad;		
10.	Scrutiny mechanism	**Compiled by** Shashank Kr Mishra, OIBMD (ECSA)	**Reviewed by** DH (OIBMD) Ocean Product Manager(NICES)	**Approved** DD (ECSA)
11.	Originating unit	OIBMD, ECSA, NRSC		
12.	Sponsor (s) / Name and Address	NRSC, Balanagar, Hyderabad		
13.	Date of Initiation	Nov, 2017		
14.	Date of Publication	Jan, 2018		

15.

Abstract: The ocean surface currents are estimated from satellite observations of surface wind from SCATSAT-1 and Sea Surface height of SARAL AltiKa. The Ekman Surface current estimated from wind stress components of SCATSAT and geostrophic current estimated form SARAL AltiKa are combined to generate ocean surface currents. The data sets are available since October, 2016. The products are validated with AVISO, OSCAR and buoy observations indicating a good relationship between the observations.

Key Words: Ocean surface current, Ekman surface current, Geostrophic current, Indian Ocean, Sea Surface Height.

Contents

1. Abstract

The ocean surface currents are estimated from satellite observations of surface wind from SCATSAT-1 and Sea Surface height of SARAL AltiKa. The Ekman Surface current estimated from wind stress components of SCATSAT and geostrophic current estimated form SARAL AltiKa are combined to generate ocean surface currents. The data sets available since October 2016. The products are validated with AVISO, OSCAR and buoy observations indicating a good relationship between the observations.

2. Introduction

The regular estimates of ocean currents are of vital importance to many oceanographic applications like ship routing, oil-spills and pollutant transport, climatic studies etc. In this regard, the observations from Indian Space Research Organisation (ISRO) SCATSAT-1 and SARAL-AltiKa altimeter are important in the estimation of ocean currents at regional and global scales. We use the data of sea surface height from SARAL-ALTIKa, ocean surface winds from SCATSAT to generate products related to ocean surface currents at the spatial resolution of 0.25° x 0.25° on a daily basis for the global ocean.

The document provides details on estimation of Ekman Currents, Sea Surface Height, Geostrophic Currents and Total Currents using SCATSAT and AltiKa data. SCATSAT and AltiKa (only for Indian Users) data products can be acquired from the web sites of the NRSC (Hyderabad) and Space Application Centre (SAC) MOSDAC (Ahmadabad). The AltiKa data is also available on AVISO ftp server for global users. The description of the products used for the estimation of ocean surface currents as well as the results along with methodology and validation are discussed in later sections. The document also provides products description and file details with naming convention and format.

3. Data and Methods

Two primarily components of the ocean surface current are namely, the wind-driven currents and the geostrophic currents (Stommel, 1960; Price et al., 1987; Sundre and Morrow, 2008). The wind-driven currents have been derived using SCATSAT wind data following the method developed by Ekman and adopted by Bonjean and Lagerloef (2002). While the geostrophic currents is derived using Saral-AltiKa sea surface height estimations. A brief description of the SARAL-AltiKa satellites has been provided below.

3.1 Saral/AltiKa Products

The Satellite with ARGOS and ALTIKA (SARAL) is a joint Indo-French satellite mission for oceanographic studies, which was launched on 25th February, 2013 from Satish Dhawan Space Centre, Sriharikota.

The AltiKa payload, built by French National Space Agency CNES, consists of a high-resolution single frequency altimeter (Ka-band), a dual frequency radiometer, Laser Retro reflector Array (LRA) and Doris. The 35.75 GHz AltiKa altimeter is the first oceanography altimeter to operate at such a high frequency. The foremost advantage of Ka-band is that it does not need second frequency to correct for ionospheric delay. The Ka-band altimeter also provides better vertical resolution (~ 0.3 metres) and smaller footprint (around 8 km). The dual frequency (24 and 37 GHz) radiometer allows for wet troposphere corrections in altimeter measurements.
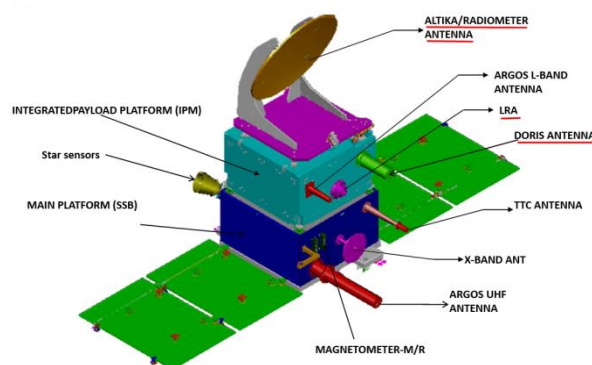

Figure 1: Saral instruments (AltiKa payload highlighted in red). (Source - AVISO)

3.2   SCATSAT

SCATSAT-1 is an OceanSat-2 follow-up mission, actually a gap-filler mission between OceanSat-2 and 3, at ISRO with the objective to continue the global ocean wind vector data acquisition started by the OSCAT (OceanSat-2 Scanning scatterometer) was launched in September 2016. The information of global ocean surface winds is an important ingredient for weather forecast.

3.3   Wind Stress

The horizontal force of the wind on the sea surface is called the **wind stress**, denoted by τ. It can also be defined as the tangential (drag) force per unit area exerted on the surface of the ocean (earth) by the adjacent layer of moving air.

To estimate surface wind stress (τ) for each scatterometer wind value, the following relation based on has been used:

$$\tau = \rho C_D W^2$$

Zonal and Meridional wind stress components are computed as:

$$\tau_X = \rho_{air} C_D W^2 \sin\theta \qquad \tau_y = \rho_{air} C_D W^2 \cos\theta$$

Where,

ρ is the density of air (1.2 kg/m^3).

C_D is a dimensionless coefficient called **drag coefficient.**

W is the wind speed.

θ is the angle of the wind vector from true north.

Drag coefficient depends on the roughness of the surface and the lapse rate. The drag coefficient C_D for the ocean surface has a non-linear relation with the wind speed, which generally increases with wind speed.

$C_D =$ **0.00218**   **W (wind speed) $\leq$ 1m/s**

(0.62 + 1.56/W)×0.001   **1 m/s < W < 3 m/s**

0.00114   **3 m/s < W < 10 m/s**

(0.49 + 0.065W)×0.001   **W $\geq$ 10 m/s**

4. Ocean Surface Currents

The Ocean surface currents are one of the dynamical features which need continuous investigation owing to their important role in various geophysical phenomena such as the transport of heat, El Nino etc. Given the large scale varying nature of currents, it is challenging to derive the current features from satellite observations. Total surface currents are primarily composed of wind driven Ekman currents and pressure gradient driven geostrophic currents.

For the computation of Ekman currents, daily composites of SCATSAT wind products have been used generated using DIVA (Data Interpolation and Variational Analysis). The wind composites are available for the Global Ocean at the spatial resolution $0.5^o \times 0.5^o$ and of $0.25^o \times 0.25^o$. After the launch of SCATSAT-1 in September 2016, the total currents have been estimated for the period of October 2016 to April, 2017. Geostrophic currents have been estimated at the spatial resolution of $0.25^o \times 0.25^o$ using Sea Surface Height (SSH) data from Saral AltiKa.

4.1 Ekman Currents

The wind-driven currents (or Ekman currents) are the resultant of frictional force exerted by wind on the ocean surface (Price et al., 1987; and Ralph and Niiler, 1999). The wind blows across the ocean and moves its waters as a result of its frictional drag on the surface. Ripples or waves cause the surface roughness necessary for the wind to couple with surface waters. Once the wind sets surface waters in motion as a current, the Coriolis Effect, Ekman transport, and the configuration of the ocean basin (topography) modify the speed and direction of the current. There are two-components of a wind driven current, a directly-driven Ekman component and an indirect component, due to the divergences and convergences of the Ekman transport that either leads to water piling up, creating a high pressure system in the ocean or to a low pressure system where surface waters diverge.

4.2 Geostrophic Currents

Geostrophic currents are the result of horizontal pressure gradient force and Coriolis force. Because of the Coriolis force, the current direction is perpendicular to the pressure gradient.

In the *f*-plane, geostrophic currents are proportional to the height gradient divided by the Earth's rotation parameter f, which is the lowest-order balance for quasi-steady circulation at higher latitudes [*Pedlosky, 1979*]. Whereas in the *β*-plane, geostrophic balance requires special attention as f tends to 0 towards the equator. As shown in different studies, *β*-plane geostrophic approximation involving the second derivative of surface heights provides excellent agreement with the observed velocity field [*Lukas and Firing, 1984*; *Picaut et al., 1989*].

4.3   Total Surface Currents

The Ekman and Geostrophic components are combined together in their respective zonal and meridional segments to obtain total currents. This provides a vector product of the ocean surface current which is represented in scatter and direction components for visualization. The data products are available as zonal and meridional components of the current. In this section, an elaborate description of data products and methodology is provided.
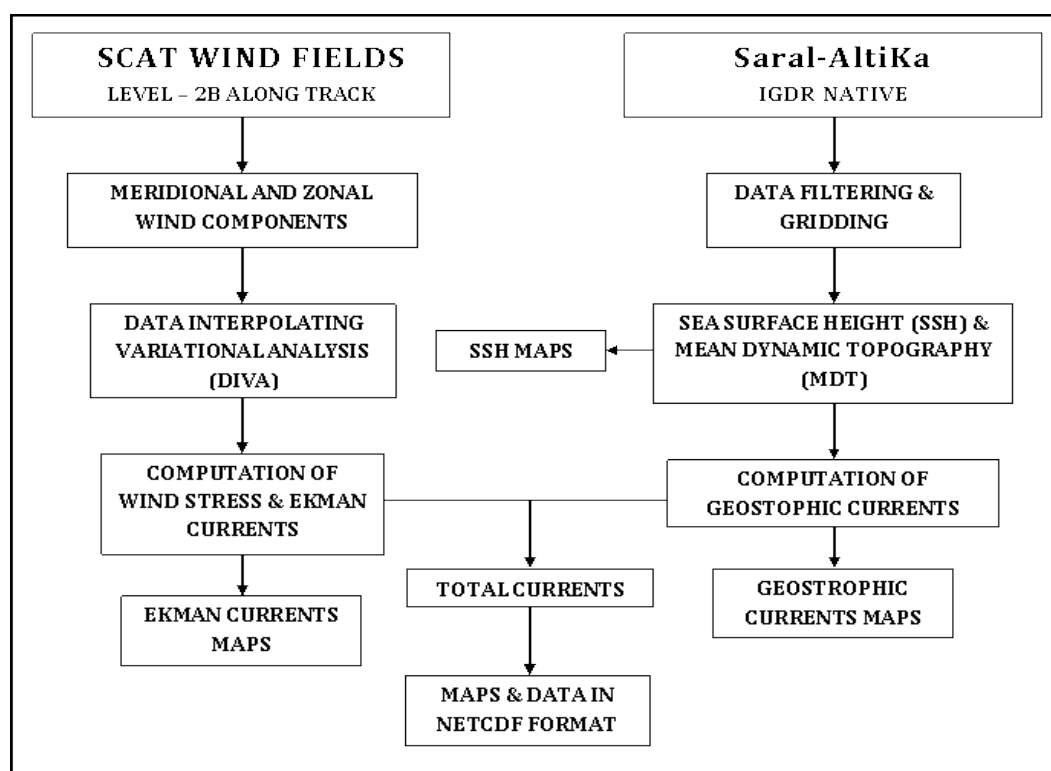
Figure 2: Flow diagram of the Currents estimation using SCATSAT & Saral-AltiKa data.

The output data files are available in NETCDF (.nc) format. The images for gridded SSH, Ekman currents, Geostrophic currents and Total currents are provided in PNG image format.

Gridded SSH has been computed using previous 15-days along track Saral-AltiKa OGDR and GDR products (Description is provided in next section). Figure 2 presents the flow diagram of the procedure followed for generation of daily products.

4.4   Nomenclature

Input and output file naming conventions are mentioned below:

Input file:
- SCATSAT-L 2B: S1L2BYYYYDDD_NNNNN_MMMMM.h5
- AltiKa   GDR:SRL_GPN_2PTPCCC_PASS_YYYYMMDD_$*^1$_ YYYYMMDD_$*^2$.CNES.nc

Output data file:
- Total Currents :   SRLP_TTT_YYYYMMDD.nc
- Geostrophic Currents :   SRLP_TTT_YYYYMMDD.nc

Output images:
- Ekman Currents: OC2S_TTT_YYYYMMDD^1_ YYYYMMDD^2.png
- Geostrophic Currents: SRLP_TTT_ YYYYMMDD^1_ YYYYMMDD^2.png
- Sea Surface Height: SRLP_TTT_ YYYYMMDD^1_ YYYYMMDD^2.png
- Total Currents: SRLP_TTT_ YYYYMMDD^1_ YYYYMMDD^2.png

Where,
- YYYY : The calendar year when data was acquired.
- MM : The month when data was acquired.
- DD : The day of the month when data was acquired.
- DDD : The day of the year when data was acquired.
- YYYYMMDD^1: Start Day (first day)
- YYYYMMDD^2: End Day (last day)
- $*^1$: Data acquisition start time (HHMMSS).
- $*^2$: Data acquisition end time (HHMMSS).
- P :   G   →   GDR

  I   →   IGDR

  O   →   OGDR
- TTT : Product Type

  TSC   →   Total Surface Currents

  GEO   →   Geostrophic Currents

  EKM   →   Ekman Currents

  SSH   →   Sea Surface Height

For more information on SCATSAT products, visit http://www.nrsc.gov.in/ and for Saral-AltiKa products, visit http://www.aviso.oceanobs.com/.

4.5   Data Processing Steps

The methodology for obtaining surface currents from satellites involves effectively and efficiently combining the Sea Surface Height (SSH) or Absolute Dynamic Topography (ADT) data from altimeters with the wind velocity data from scatterometers. All the current products are generated for the Global Ocean. MATLAB tools have been used for the computation and generation of output products. The following steps have been adopted for the derivation of products:

Estimation of Ekman Currents:

For the wind-driven (Ekman) currents, the Ekman components (u_e, v_e) are given by [*Van Meurs & Niiler*, 1999]:

$$u_e + iv_e = Be^{i\varphi}(\tau_x + i\tau_y);$$

$$B = \frac{1}{\rho}(r^2 + f^2h^2)^{-\frac{1}{2}}, \varphi = arctan\left(\frac{fh}{r}\right)$$

.................(1)

Where [u_e, v_e] are the zonal and meridional ekman current components, respectively. ρ is the density of water (1025 kgm^{-3}), h is the wind mixing depth and r is a linear drag coefficient that represents vertical viscosity terms. τ_x and τ_y represent the Wind stress components, which have been directly taken from the products available at NICES portal of Bhuvan website. These stress components are computed as:

$$\tau_x = \rho_{air}C_DW^2sin\theta \qquad \tau_y = \rho_{air}C_DW^2cos\theta$$

..........................(2)

Where, C_D is a dimensionless coefficient called drag coefficient. Non-linear drag coefficient (C_D) based on Large & Pond (1981) modified for low wind speeds [Trenberth et al., 1990] is used. W is the wind speed (taken from Daily Wind Composites products available at NICES portal), θ is the angle of wind vector from true north and ρ is the density of air (1.2 kg/m^3).

Finally it comes out to be:

$$u_e = \frac{1}{\rho(r^2 + f^2h^2)}(r\tau_x + fh\tau_y)$$

$$v_e = \frac{1}{\rho(r^2 + f^2h^2)}(r\tau_y - fh\tau_x)$$

.................(3)

Lagerloef et al. (1999) performed a regression analysis and found values of $r = 2.15 \times 10^{-4}$ ms^{-1} and $h = 32.5$ m, which remain fairly constant over the tropical band. We have used the same values in our analysis.

Gridding of SSH and MDT:

SSH and MDT data has been gridded at a spatial resolution of 0.25°×0.25° for the complete global scale. For gridding, Saral-AltiKa GDR native data set for the last 15 days has been filtered and then, accumulated for each 0.25° grid cell and the median value is allotted to that particular grid cell. SSH is defined at the sum of Sea Surface Height Anomaly (SSHA) and MDT. For accumulation, all the observations lying within a latitudinal separation of 0.125 degrees and longitudinal separation of 0.5 degrees from each grid cell are taken.
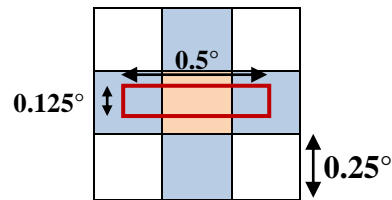
The filtering of the data has been carried out as per the conditions provided by the document available at AVISO website:

After applying all the above mentioned filters and flags, median of all the observations (from last 15 days) lying within 0.25° of each grid cell is allotted to that particular cell. This gridded SSH and MDT is further smoothed using moving average technique with the window of 1.25° x 1.25° (i.e. 5 x 5 grid cells).

Estimation of Geostrophic Currents:

From this absolute dynamic topography, the geostrophic currents are then to be computed as the gradient of ADT. In the f-plane, the two components i.e. east and north ($u_{g,f}$, $v_{g,f}$) of the surface geostrophic current vector are then given as:

$$u_{g,f} = -\frac{g}{f}\frac{\partial \zeta}{\partial y}, \qquad v_{g,f} = \frac{g}{f}\frac{\partial \zeta}{\partial x} \qquad \text{...........................(4)}$$

Where, g is the acceleration due to gravity, f is the Coriolis parameter ($f = 2\,\Omega \sin \varphi$), and ζ is the height of the sea surface above a level surface (ADT). φ is the latitude and Ω is the angular velocity of the earth's rotation ($\Omega = 7.29\text{x}10^{-5}$ sec^{-1}).

In the β-plane, as shown by Lagerloef at al. (1999) the geostrophic currents ($u_{g,\beta}$, $v_{g,\beta}$) are computed as:

$$u_{g,\beta} = -\frac{g}{\beta}\frac{\partial^2 \zeta}{\partial^2 y}, \quad v_{g,\beta} = \frac{g}{\beta}\frac{\partial^2 \zeta}{\partial x \partial y}$$ ....(5)

where, $\beta = \frac{\partial f}{\partial y}$.

For the equatorial region, β is a constant given by $\beta = 2\,\Omega/r = 2.3 \text{ x } 10^{-11}$ m^{-1}s^{-1}. Picaut et al. (1989) also state that the second derivative is valid over spatial scales of > 100 km and timescales greater than 15-30 days, providing relatively smoothed geostrophic velocities at the equator. The computation of Geostrophic currents in the equatorial region requires further investigation.

The final currents are then a linear combination of geostrophic and wind-driven (Ekman) motion given as:

$$\bar{U} = \bar{U}_g + \bar{U}_e$$ ....(6)

where, $\bar{U}_g$ and $\bar{U}_e$ are the Geostrophic and Ekman components, respectively.

5. Results and Discussion

The Saral-AltiKa and scatterometers derived ocean surface currents have been compared with CNES AVISO geostrophic currents and NOAA OSCAR total currents for the year 2013 (i.e. 28th Mar, 2013 to 31st Dec, 2013). Both the AVISO and OSCAR currents data are available at spatial resolution of 0.33° with temporal resolution of daily and 5 days respectively. The datasets are regridded to the spatial resolution of 0.25° using nearest neighborhood method. The results have been indicated. The validation of the currents is still in progress, but the preliminary results are very promising. The comparisons are also carried out at different spatial and temporal resolutions.

5.1 Comparison with AVISO Geostrophic currents

The comparison results of Saral-AltiKa derived geostrophic currents with AVISO geostrophic currents are shown in Tables 1 & 2. As can be seen, geostrophic currents in f-plane show better correlation than those in β-plane. This can be attributed to Coriolis parameter which approaches zero in the β-plane. Also, the zonal component of geostrophic currents shows better correlation than meridional component. The bias in currents speed (f-plane) varies in the range of 3.5 – 4.5 cm/s. The correlation is highest for the months of April. As the products are still in testing phase, it will be difficult to comment on the causes of these discrepancies.

Month	R_U	R_V	R_W
Nov (2016)	0.44	0.31	0.35
Dec(2016)	0.51	0.35	0.42
Jan(2017)	0.60	0.29	0.45
Feb(2017)	0.57	0.39	0.44
Mar|(2017)	0.62	0.32	0.46
Apr(2017)	0.60	0.40	0.49

Table 1: AVISO versus Saral-AltiKa derived geostrophic currents for 2016-17. Monthly mean values of correlation coefficient (R) has been indicated for zonal (U), meridional (V) and total (W) currents.

Month	R_U	R_V	R_W
Nov (2016)	0.61	0.44	0.50
Dec(2016)	0.60	0.42	0.50
Jan(2017)	0.68	0.44	0.51
Feb(2017)	0.68	0.42	0.55
Mar|(2017)	0.77	0.50	0.61
Apr(2017)	0.71	0.56	0.63

Table 2: AVISO versus Saral-AltiKa derived geostrophic currents in the f-plane (|latitude| > 5) for 2016-17. Monthly mean values of correlation coefficient (R) have been indicated for zonal (U), meridional (V) and total (W) currents.

5.2   Comparison with OSCAR total currents

The comparison results of Saral-AltiKa and scatterometer derived total currents with OSCAR geostrophic currents are shown in Table 3 & 4. As was observed in the case of AVISO, currents in f-plane show better correlation than those in β-plane. Also, the zonal component of currents shows better correlation than meridional component. The bias in currents speed (f-plane) has now reduced to the range of 1 – 3 cm/s. In this case also, the correlation is highest for the month of April.

.

Month	R_U	R_V	R_W
Nov (2016)	0.54	0.37	0.56
Dec(2016)	0.60	0.40	0.60
Jan(2017)	0.67	0.47	0.61
Feb(2017)	0.62	0.47	0.58
Mar|(2017)	0.59	0.46	0.56
Apr(2017)	0.67	0.42	0.62

Table 3: OSCAR versus Saral-AltiKa derived total currents for 2016-17. Monthly mean values of correlation coefficient (R) have been indicated for zonal (U), meridional (V) and total (W) currents.

Month	R_U	R_V	R_W
Nov (2016)	0.72	0.54	0.54
Dec(2016)	0.70	0.49	0.54
Jan(2017)	0.72	0.47	0.55
Feb(2017)	0.77	0.51	0.58
Mar|(2017)	0.78	0.53	0.64
Apr(2017)	0.81	0.57	0.68

Table 4: OSCAR versus Saral-AltiKa derived total currents in the f-plane (|latitude| > 5) for 2016-17. Monthly mean values of correlation coefficient (R) have been indicated for zonal (U), meridional (V) and total (W) currents.
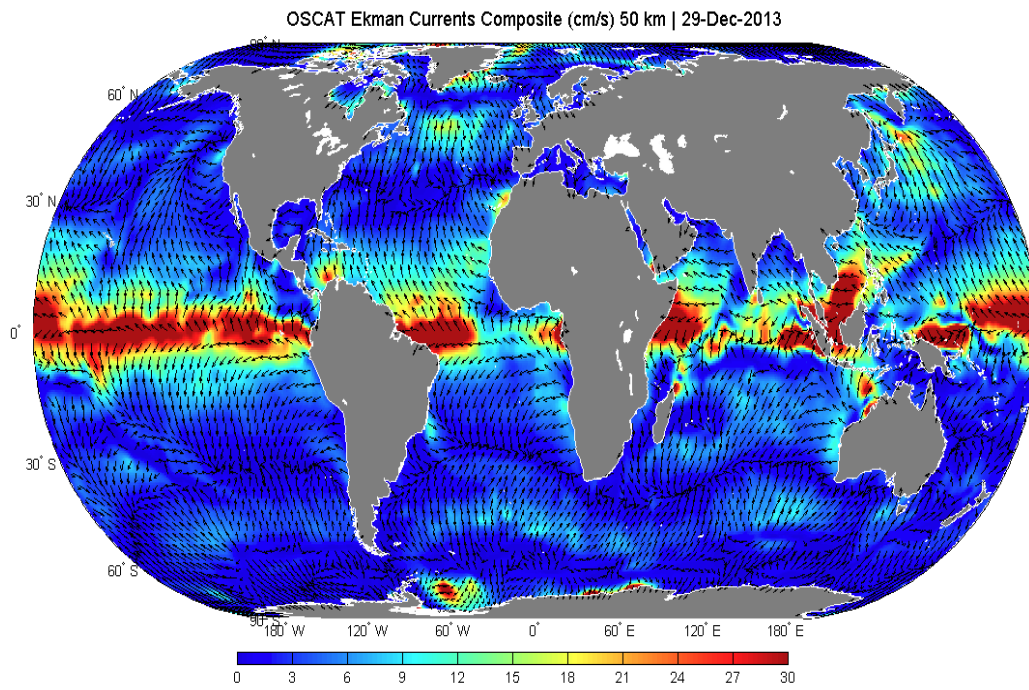
6. Sample Products

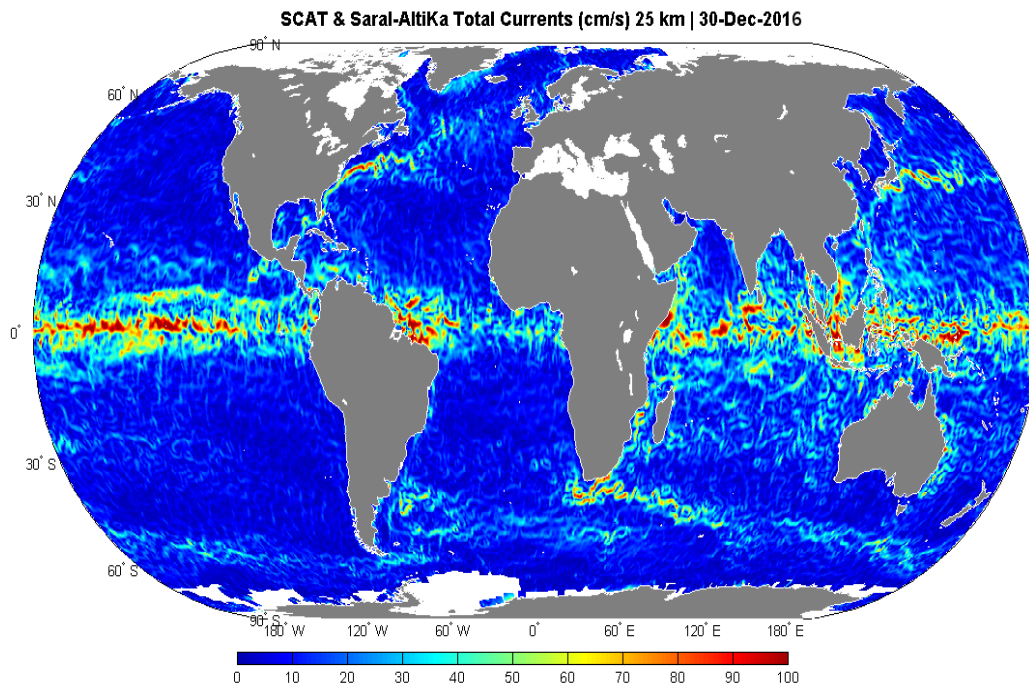**Figure 3: OSCAT derived Ekman Currents for global Ocean.**

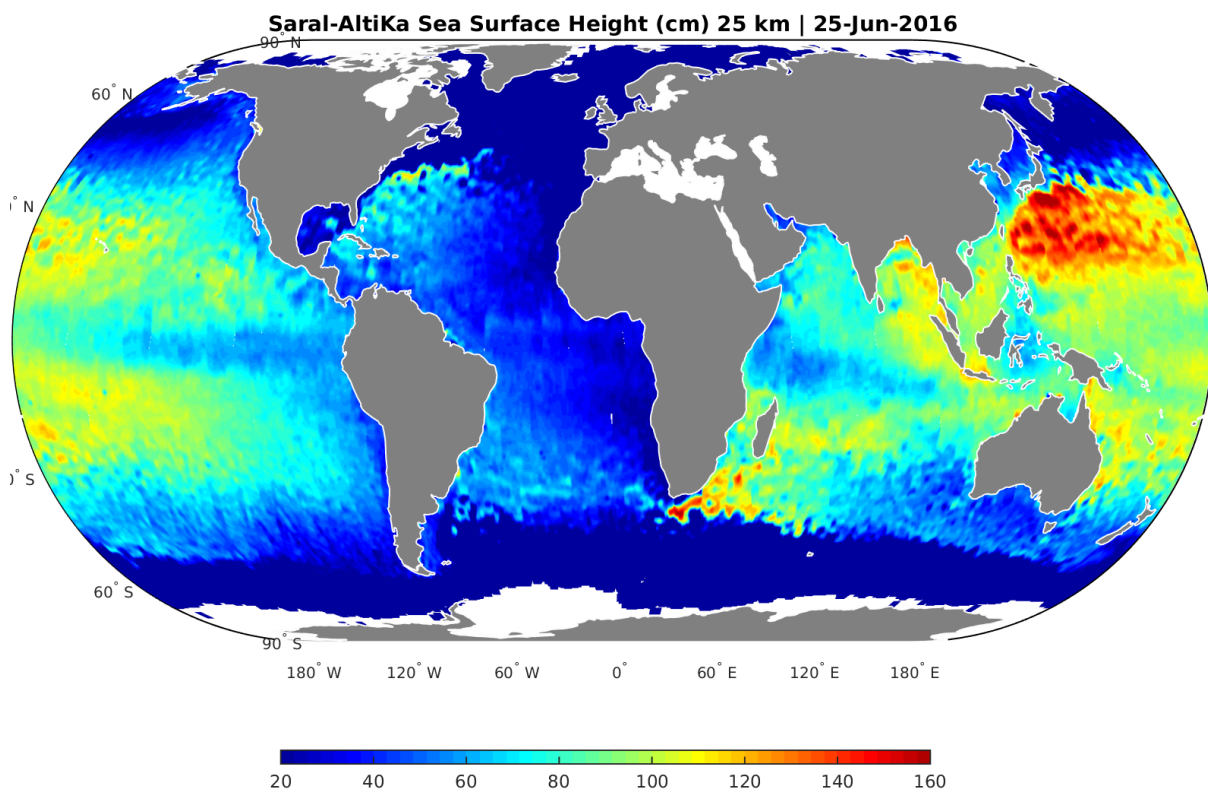**Figure 4: SCATSAT and SARAL derived Total Surface Currents for global Ocean.**

Saral-AltiKa Sea Surface Height (cm) 25 km | 25-Jun-2016

Figure 5: SARAL derived Sea Surface Height for global Ocean.

Saral-AltiKa Geostrophic Currents (cm/s) 25 km | 25-Jun-2016
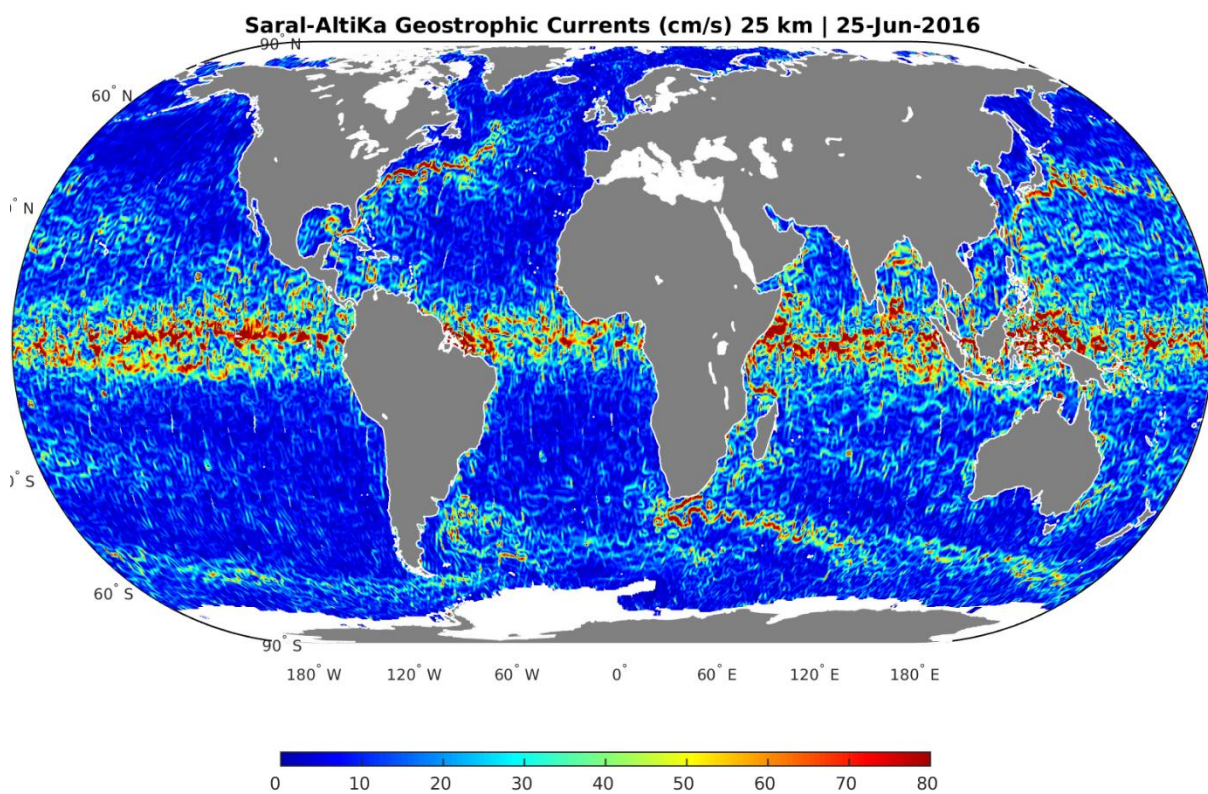
Figure 6: SARAL derived Geostrophic Currents for global Ocean.

7. Conclusion

The ocean surface currents derived using products of SCATSAT and Saral-AltiKa show very promising results. The salient features of Indian Ocean circulation, with seasonal variations are reflected in the total surface currents. Major gyre systems and general circulation pattern in the Indian Ocean region can be easily distinguished. Also, the preliminary validation results at different spatial and temporal resolutions with INCOIS buoys show promising correlation coefficient (R^2) ranging from 0.42 to 0.59. Bias for zonal currents is more negative (≈ -5 cm/s) than that for meridional component (≈ -3 cm/s). There is a scope for better results by performing global validation and fine tuning of algorithm.

8. References

AVISO User Handbook Ssalto/Duacs: M(SLA) and M(ADT) Near-Real Time and Delayed-Time, *SALP-MU-P-EA-21065-CLS*, edition 4.1, May 2014 (AVISO - Archiving, Validation and Interpretation of Satellite Oceanographic Data) www.oceanobs.aviso.com

Bonjean, F. and Gary S. E. Lagerloef (2002), Diagnostic model and analysis of the surface currents in the tropical Pacific ocean, *J. Phys. Oceanogr.*, 32, 29382954.

Dorandeu, J. and P. Y. Le Traon (1999), Effects of global mean atmospheric pressure variations on mean sea level changes from TOPEX/Poseidon, *J. Atmos. Oceanic Technol.*, 16, 1279–1283.

Ducet, N., P. Y. Le Traon and G. Reverdin (2000), Global high resolution mapping of ocean circulation from TOPEX/Poseidon and ERS 1 and 2, *J. Geophys. Res.*, 105 (C8), 19,477-19,498.

Lagerloef, G. S. E., G. T. Mitchum, R. Lukas and P. P. Niiler (1999), Tropical pacific near surface currents estimated from altimeter, wind and drifter data, *J. Geophys. Res.*, 104, 23,313–23,326.

Le Traon, P.-Y. and F. Ogor(1998), ERS-1/2 orbit improvement using TOPEX/Poseidon: The 2 cm challenge, *J. Geophys. Res.*, 103, 8045–8057.

Lukas, R. and E. Firing, 1984: The geostrophic balance of the Pacific Equatorial Undercurrent, Deep-Sea Res., 31, 61–66.

OSCAT Product Handbook, Version 1.3, Dec. 2011.

Price, J. F., R. A. Weller and R. R. Schudlich (1987), Wind-Driven Ocean Currents and Ekman Transport, *Science*, 238 (4833), 1534-1538.

Geophysical fluid dynamics, Joseph Pedlosky. Springer-Verlag, Berlin,1979

Philander, S. G. H. and R. C. Pacanowski (1980), The generation of equatorial currents, *J. Geophys. Res.*, 85, 1,123–1,136.

Picaut J, Hayes SP, McPhaden MJ (1989) Use of the geostrophicapproximation to estimate time-varying zonal currents at theequator. J Geophys Res 94:3228–3236.

Ralph, E. A. and P. P. Niiler (1999), Wind-driven currents in the tropical pacific, *J. Phys. Oceanogr.*, 29, 2121–2129.

Saral-AltiKa Products Handbook, *SALP-MU-M-OP-15984-CN*, Issue 2.3, July 2013.

Seidel HF, Giese BS (1999) Equatorial currents in the Pacific Ocean1992–1997. J Geophys Res 104:7849–7863

Stommel, H. (1960), Wind-drift near the equator, *Deep Sea Res.*, 6, 298–302.

Sudre,J. and R. Morrow (2008), Global surface currents: a high-resolution product for investigating ocean dynamics, *Ocean Dynamics*, DOI 10.1007/s10236-008-0134-9.

K.E. Trenberth, W.G. Large & J.G. Olson, 1990, "The Mean Annual Cycle in Global Ocean Wind Stress", *J.Physical Oceanography*, Vol. 20, pp. 1742 – 1760.

Van Meurs P, Niiler PP (1997), Temporal variability of the large-scale geostrophic surface velocity in the northeast Pacific, *J. Phys. Oceanogr.,* 27:2288–2297

W. G. Large & S. Pond., 1981,"Open Ocean Measurements in Moderate to StrongWinds", *J. Physical Oceanography*, Vol. 11, pp. 324 - 336.